Supplementary Information (SI) for Green Chemistry.

Supporting Information

Covalent organic framework-derived highly dispersed Pt single atoms collaborate with Pt nanoclusters electrocatalyst for acid hydrogen evolution

Huihui Zhao,[a]† Xinghao Zhang,[c]† Chengcheng Yu,[a]† Wenya Gao,[a] Xiuxiu Chen,[b] Haikuo Lan,[a] Xiaorong Xin,[a] Kang Liu,[a] and Dingxuan Ma*[a]

[a] College of Chemistry and Molecular Engineering, Key Laboratory of Optic-electric Sensing and Analytical Chemistry for Life Science, Shandong Key Laboratory of Biochemical Analysis, Qingdao University of Science and Technology, Qingdao 266042, P. R. China.

[b] College of Chemical Engineering, Qingdao University of Science and Technology, Qingdao 266042, PR China.

[c] School of Materials Science and Engineering, Nankai University, Tianjin 300350, P. R. China.

E-mail: madingxuan640@126.com

† These authors contributed equally to this work.

1. Materials and Reagents

Ethidium bromide (99%), 1,3,5-triformylphloroglucinol (98%), sodium dicyanamide (97%) and potassium tetrachloroplatinate (98%) were bought from Adamas. Pt/C (20%) was bought from Alfa. Ethanol (99.9%) and sulfuric acid (95~98%) were bought from Sinopharm Chemical Reagent Co., Ltd. All reagents were used without further purification. The monodisperse PS spheres were synthesized according to the previous literature.[1]

2. Instrumentation

The Powder X-ray diffraction (PXRD) was performed by Rigaku D/MAX2550 diffractometer. The scanning electron microscopy (SEM) and transmission electron microscopy (TEM) were used to characteristic the morphology by JSM-7500F and the FEI Tecnai G2 S-Twin with a field emission gun operating at 200 kV. Gas adsorption experiments were adopted by Micrometrics ASAP 2020M volumetric gas adsorption analyzer. Inductively coupled plasma-optical emission spectrometry (ICP-OES) was carried out on an Agilent 730. Raman spectra were measured by inVia Reflex. X-ray photoelectron spectroscopy (XPS) was measured on an ESCALAB 250 X-ray photoelectron spectroscopy using Mg Kα X-ray as the excitation source. Aberration-corrected high-angle annular dark-field scanning transmission electron microscopy (AC-HAADF-STEM) was conducted using a JEM-ARM 200F microscope operating at 300 kV.

3. Synthetic Procedures

3.1 Synthesis of PS@EB-COF:Br. EB (0.225 mmol), p-touenesulfonic acid (1.45 mmol) and 2.5 mL colloidal PS were mixed thoroughly in a vortex shaker. Then Tp (0.15 mmol) was added into above mixed solution and further stirring for 30 min. The mixtures were poured into an open petri dish to evaporate water. And the obtained solid sample was heated at 80°C for 24 h. The solid was washed with water and ethanol. The PS@EB-COF:Br was obtained after drying overnight in a vacuum oven at 60 °C.

3.2 Synthesis of PS@EB-COF:DCA-Pt_1. 257 mg of PS@EB-COF:Br was dispersed in a 10 mL solution of NaDCA (0.09 mol/L) and stirred for 4 h. Subsequently, the solution was filtered, and this process was repeated twice to obtain the PS@EB-COF:DCA precursor. Then the obtained solid sample was stirred in a 5 mL solution of potassium tetrachloroplatinate (0.2 mg/mL) at room temperature for 12 h to synthesis the PS@EB-COF:DCA-Pt_1.

3.3 Synthesis of mCN-Pt_1. PS@EB-COF:DCA-Pt_1 was placed in a small ceramic boat inside a tube furnace under a nitrogen atmosphere. The sample was calcined at 900 °C for 3 h with a ramp rate of 5 °C/min. After cooled naturally to room temperature, mCN-Pt_1 can be obtained. The synthetic process of mCN-Pt_{700} and mCN-Pt_{800} was similar to that of mCN-Pt_1 except that the annealed temperatures are 700 °C and 800 °C.

3.4 Synthesis of mCN-Pt_2. The synthetic process was similar to that of mCN-Pt_1 except that the concentration of the potassium tetrachloroplatinate solution was 0.6 mg/mL.

3.5 Synthesis of mCN-Pt_{NP}. The synthetic process was similar to that of mCN-Pt_1 except using PS@EB-COF:Br instead of PS@EB-COF:DCA as precursor.

3.6 Synthesis of mCN-Pt_{SA}. The synthetic process was similar to that of mCN-Pt_1 except that the PS@EB-COF:DCA precursor was stirred in a 20 mL solution of potassium tetrachloroplatinate (0.05 mg/mL).

3.7 Synthesis of mCN-Pt_{NC}. PS@EB-COF:DCA precursor was calcined at 900

°C for 3 h with a ramp rate of 5 °C/min in nitrogen atmosphere. After cooled naturally to room temperature, the sample was stirred in a 5 mL solution of potassium tetrachloroplatinate (0.2 mg/mL) at room temperature to synthesis the precursor. The precursor was treatment at 300 °C for 2 h in 5% H_2/Ar. After cooled naturally to room temperature, mCN-Pt_{NC} can be obtained.

3.8 Synthesis of CN-Pt. EB-COF:Br was obtained according to the previous literature.[2] This compound served as a precursor, and the specific synthesis method employed is similar to that of mCN-Pt_1. Ultimately, the CN-Pt sample was obtained without the involvement of the PS template.

4. Electrochemical measurements

All electrochemical tests were measured by the CHI760E electrochemical work station. The typical three-electrode system was adopted, which the glassy carbon electrode (GC) with the diameter of 3 mm as working electrode, the graphite rod as counter electrode and the saturated calomel electrode (SCE) as reference electrode. All potentials were calibrated to the reversible hydrogen electrode (RHE) scale by the following equation: $E_{RHE} = E_{RE} + 0.059 \times pH + E_{RE}^0$.

In a typical preparation of the catalyst ink, 5 mg of each catalyst was dispersed in 560 μL of ethanol, 400 μL of water and 40 μL of 5 % Nafion mixed solution, followed by ultrasonication. Subsequently, 5 μL catalyst ink was dropped on the glassy carbon electrode to form a catalyst film with a catalyst loading of 0.354 mg cm^{-2}. According to the Pt content in the ICP, the Pt loading on the electrode of mCN-Pt_1 is 3.68 μg cm^{-2}. The LSV curves of HER was measured in N_2-saturated 0.5 M H_2SO_4. And the double layer capacitance (C_{dl}) was estimated by conducting the cyclic voltammetry under incremental scan rates (20, 40, 60, 80, 100, and 120 mV s^{-1}).

5. Characterization

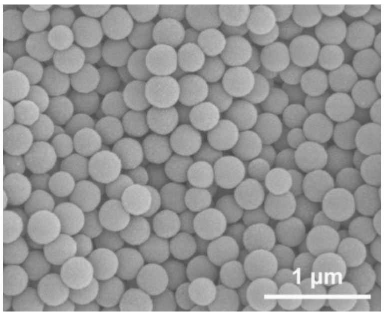

Figure S1 The SEM image of PS templates.

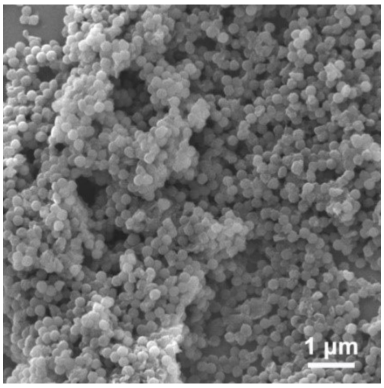

Figure S2 The SEM image of PS@EB-COF:DCA-Pt_1.

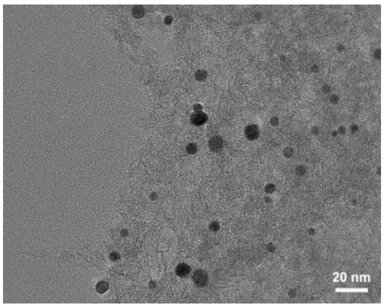

Figure S3 The TEM image of mCN-Pt_{NP}.

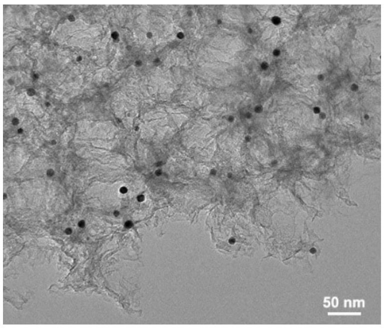

Figure S4 The TEM image of mCN-Pt_2.

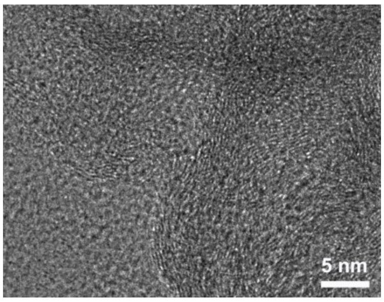

Figure S5 The TEM image of mCN-Pt_1.

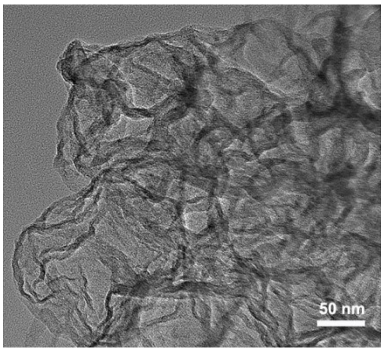

Figure S6 The TEM image of mCN-Pt_{NC}.

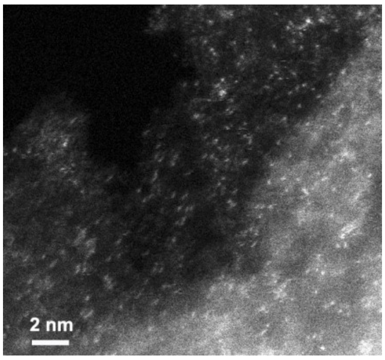

Figure S7 The HAADF-STEM image of mCN-Pt_{SA}.

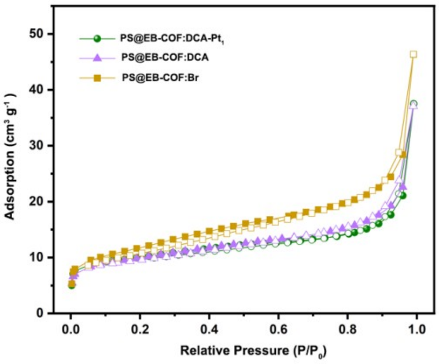

Figure S8 N_2 adsorption-desorption isotherms of PS@EB-COF:Br, PS@EB-COF:DCA, and PS@EB-COF:DCA-Pt_1.

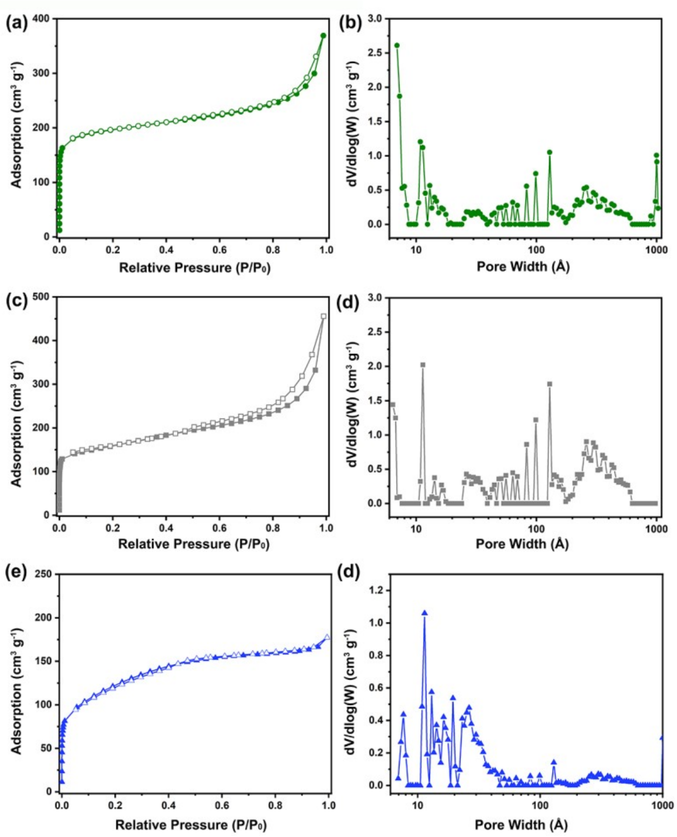

Figure S9 (a) N_2 adsorption-desorption isotherms of mCN-Pt_1; (b) Pore size distributions of mCN-Pt_1; (c) N_2 adsorption-desorption isotherms of mCN-$\mathrm{Pt}_{\mathrm{NP}}$; (d) Pore size distributions of mCN-$\mathrm{Pt}_{\mathrm{NP}}$; (e) N_2 adsorption-desorption isotherms of CN-Pt; (f) Pore size distributions of CN-Pt.

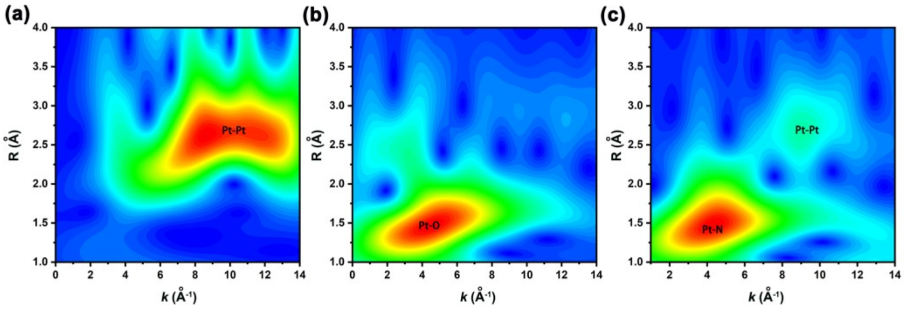

Figure S10 WT contour plots of Pt foil (a), PtO_2 (b) and mCN-Pt_1 (c).

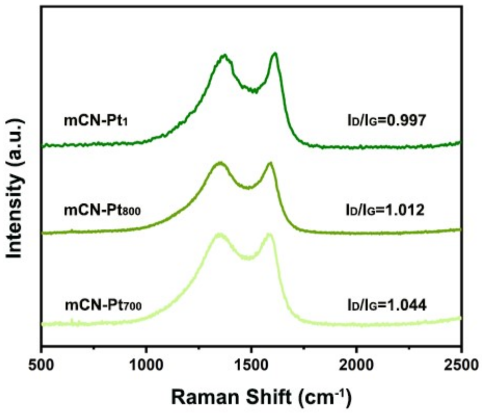

Figure S11 Raman spectra.

To investigate the effect of carbonization temperature on the sample performance, we conducted Raman spectroscopy tests on samples synthesized at 700 °C, 800 °C, and 900 °C. The Raman test results indicate that the I_D/I_G ratio decreases with increasing temperature, suggesting that the graphitization degree of the material improves as the temperature rises. This enhancement in graphitization is beneficial for improving the electrical conductivity of the material.

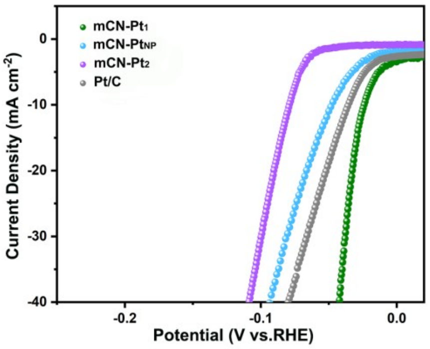

Figure S12 HER polarization curves of mCN-Pt$_1$, mCN-Pt$_2$, mCN-Pt$_{NP}$ and Pt/C.

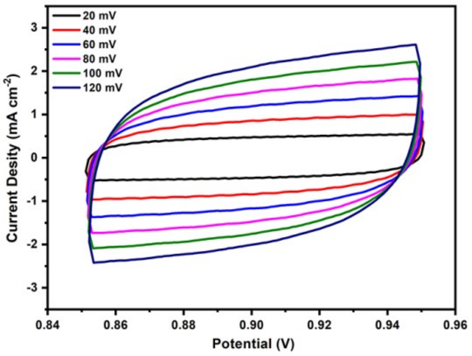

Figure S13 Cyclic voltammetry curves at different scan rates for mCN-Pt$_1$.

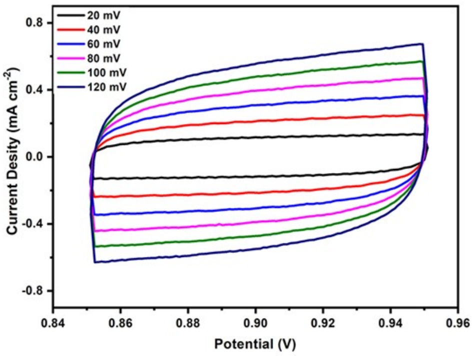

Figure S14 Cyclic voltammetry curves at different scan rates for mCN-Pt$_{NP}$.

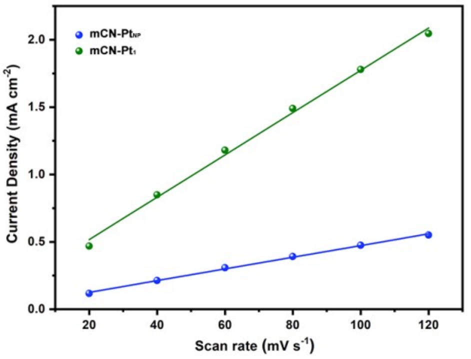

Figure S15 The corresponding linear fitting of the current density versus scan rates.

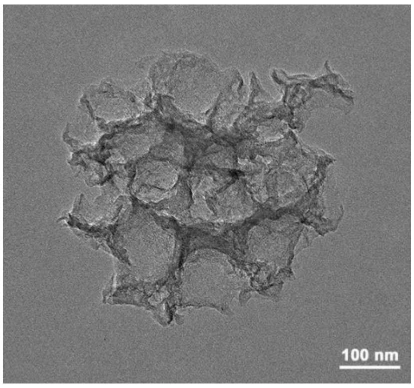

Figure S16 TEM image of mCN-Pt_1 after used.

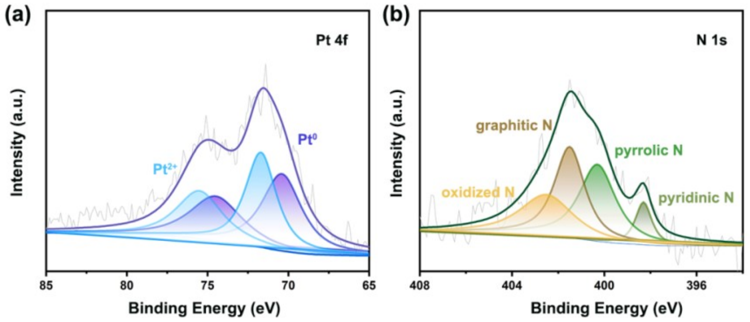

Figure S17 Pt 4f and N 1s XPS spectras of mCN-Pt_1 after used.

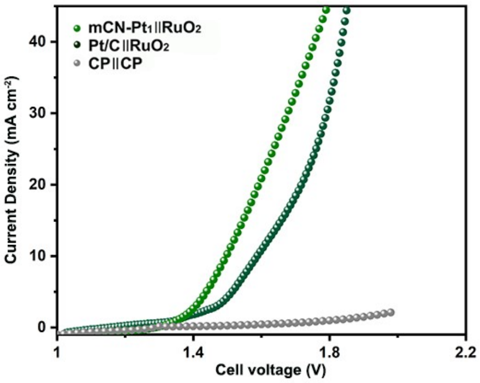

Figure S18 Polarization curves of mCN-Pt_1||RuO_2, Pt/C||RuO_2 and CP||CP in 0.5 M H_2SO_4 for water splitting.

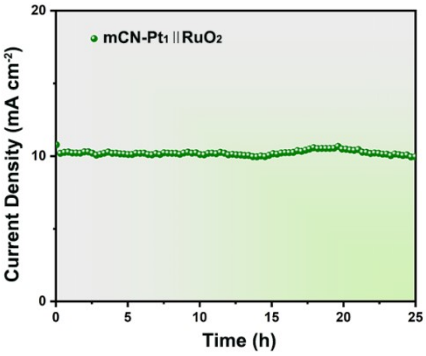

Figure S19 Chronoamperometric test for mCN-Pt_1||RuO_2 cell.

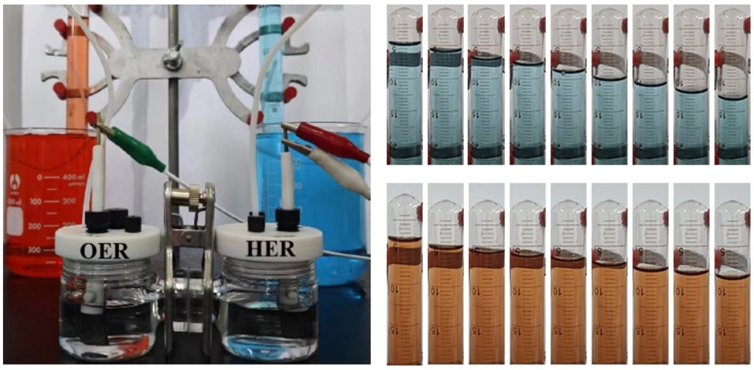

Figure S20 The device for monitoring the rates of H_2 and O_2 production.

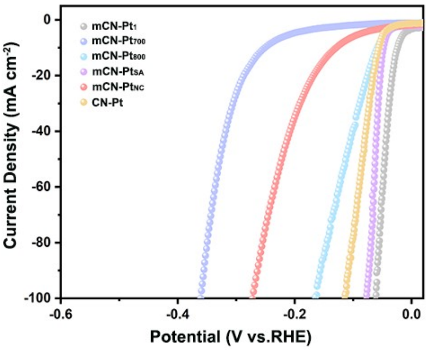

Figure S21 HER polarization curves of mCN-Pt_1 and contrast samples.

Table S1 Different element contents in mCN-Pt_1 and mCN-Pt_{NP}

Sample	C (wt%)	H (wt%)	N (wt%)
mCN-Pt_1	78.14	0.25	6.82
mCN-Pt_{NP}	82.20	0.29	5.66

6. Computational modelling

First-principles methods were employed to conduct density functional theory (DFT) calculations within the generalized gradient approximation (GGA) using the Perdew-Burke-Ernzerhof (PBE) formulation.[3-5] The projected augmented wave (PAW) potentials were selected to accurately describe the ionic cores and account for valence electrons, employing a plane wave basis set with a kinetic energy cutoff of 520 eV. [6-7] Partial occupancies of the Kohn-Sham orbitals were permitted using the Gaussian smearing method, with a width of 0.05 eV. The electronic energy was deemed self-consistent when the energy change was less than 10^{-5} eV. A geometry optimization was considered convergent when the energy change was below 0.05 eV $Å^{-1}$. The vacuum spacing in the direction perpendicular to the plane of the structure was set to 18 Å. Brillouin zone integration was performed using a 3×3×1 Monkhorst-Pack k-point sampling for the structure. The adsorption energies (E_{ads}) were calculated using the formula $E_{ads}= E_{ad/sub} - E_{ad} - E_{sub}$, where $E_{ad/sub}$, E_{ad}, and E_{sub} represent the total energies of the optimized adsorbate/substrate system, the adsorbate in the structure, and the clean substrate, respectively. The free energy was calculated using the equation:

$$G = E + ZPE - TS$$

where G, E, ZPE and TS denote the free energy, total energy from DFT calculations, zero-point energy and entropic contributions, respectively. In our calculations, the top two layers were relaxed, while the remaining layers were fixed in their surface structures. For the amorphous structure, we obtained a stable configuration at 300 K using ab initio first-principles methods.

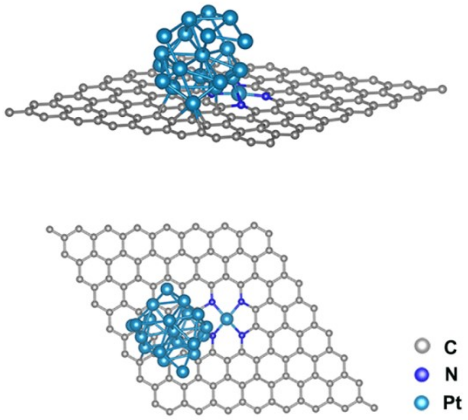

Figure S22 Side view and top view of Pt cluster/Pt-N_4.

7. References

[1] K. Shen, L. Zhang, X. Chen, L. Liu, D. Zhang, Y. Han, J. Chen, J. Long, R. Luque, Y. Li and B. Chen, *Science*, 2018, **359**, 206-210.

[2] H. Ma, B. Liu, B. Li, L. Zhang, Y. Li, H. Tan, H. Zang and G. Zhu, *J. Am. Chem. Soc.*, 2016, **138**, 5897-5903.

[3] G. Kresse and J. Furthmüller, *Comput. Mater. Sci.*, 1996, **6**, 15-50.

[4] G. Kresse and J. Furthmüller, *Phys. Rev. B* 1996, **54**, 11169-11186.

[5] J. P. Perdew, K. Burke and M. Ernzerhof, *Phys. Rev. Lett.*, 1996, **77**, 3865-3868.

[6] G. Kresse and J. Furthmüller, *Phys. Rev. B* 1996, **54**, 11169-11186.

[7] P. E. Blöchl, *Phys. Rev. B* 1994, **50**, 17953-17979.